Macroparasite dynamics of migratory host populations

Stephanie J. Peacock[a,b,c,*], Juliette Bouhours[d], Mark A. Lewis[b,d], Péter K. Molnár[a,e]

[a]*Ecology and Evolutionary Biology, University of Toronto*
[b]*Biological Sciences, University of Alberta*
[c]*Current address: Biological Sciences, University of Calgary*
[d]*Mathematical and Statistical Sciences, University of Alberta*
[e]*Biological Sciences, University of Toronto Scarborough*

Abstract

Spatial variability in host density is a key factor affecting disease dynamics of wildlife, and yet there are few spatially explicit models of host-macroparasite dynamics. This limits our understanding of parasitism in migratory hosts, whose densities change considerably in both space and time. In this paper, we develop a model for host-macroparasite dynamics that considers the directional movement of host populations and their associated parasites. We include spatiotemporal changes in the mean and variance in parasite burden per host, as well as parasite-mediated host mortality and parasite-mediated migratory ability. Reduced migratory ability with increasing parasitism results in heavily infested hosts halting their migration, and higher parasite burdens in stationary hosts than in moving hosts. Simulations reveal the potential for positive feedbacks between parasite-reduced migratory ability and increasing parasite burdens at infection hotspots, such as stopover sites, that may lead to parasite-induced migratory stalling. This framework could help understand how global change might influence wildlife disease via changes to migratory patterns and parasite demographic rates.

Keywords: macroparasite; population; animal migration; disease; partial-differential equation; spatial dynamics

1. Introduction

Many animals undergo arduous migrations to track seasonal changes in environmental conditions and resources. The resulting spatiotemporal changes in host density have profound and diverse consequences for the dynamical interactions between hosts and parasites (Altizer et al., 2011). For example, host migration may facilitate the spread of parasites into new areas where they might infect novel host species - an increasing concern in the face of warming temperatures that allow parasites to persist where they previously could not (e.g.,

*stephanie.j.peacock@gmail.com

Kutz et al., 2013). Alternately, migratory hosts may escape parasitism by moving away from infection hotspots where parasites have accumulated in the environment (Bartel et al., 2011). Such migratory escape has, for example, been proposed as a driver of post-calving migration in caribou (Folstad et al., 1991). Migratory lifecycles may also reduce transmission of parasites from adults to juveniles, termed migratory allopatry, as is the case for sea louse parasites of Pacific salmon (Krkošek et al., 2007). Mechanisms such as parasite spread and migratory escape may act simultaneously, with their relative importance depending on the life histories of both the parasite and the host. Further, changes in host-parasite dynamics due to, for example, climate change (Kutz et al., 2013) or the introduction of reservoir hosts (Krkošek et al., 2007; Morgan et al., 2007) may alter how migration influences host-parasite dynamics. These complexities make it difficult to understand and predict the how migration influences host-parasite dynamics.

Mathematical models describing the growth and spread of infectious pathogens through a host population have been integral to the understanding of disease dynamics in both human and wildlife populations (May and Anderson, 1991; Hudson et al., 2002). Two basic structures have been applied in modelling disease dynamics: (1) compartmental models typically used to describe microparasites and (2) macroparasite models. Compartmental models track the transition of hosts between susceptible (S) and infected (I) categories and thus describe the prevalence of infection within the host population. Sometimes immune or recovered (R) hosts are also considered, leading to the common designation as SIR models. These models are typically used to describe microparasites (e.g., viruses, bacteria) because the impact of the parasite is assumed to be independent of the number of parasites infecting a host (Anderson and May, 1979).

Several recent studies have used compartmental models to understand and predict parasite dynamics in migratory wildlife (e.g., Hall et al., 2014; Johns and Shaw, 2015; Hall et al., 2016). These models tracked the densities of susceptible and infected hosts at different stages in the annual cycle (e.g., breeding, migration, and overwintering). Hall et al. (2014) describe

an SI model in which mortality of host populations during migration depends on their infection status at the end of the breeding or overwintering season. They found that migration lowered pathogen prevalence via culling of infected hosts, and thus host population health improved with earlier departure and longer-distance migrations. Johns and Shaw (2015) built upon that model to look at disease prevalence in migratory vs. non-migratory populations with similar results: host populations ended up healthier if they spent more time migrating and had higher mortality during migration due to disease or other factors. More recent work on vector-borne diseases has also considered how changing phenology associated with climate change might lead to "migratory mismatch" of host and vector densities (Hall et al., 2016).

Macroparasite dynamics require a different model structure than microparasites because the impact of macroparasites on hosts is often proportional to parasite burden, as is typical for many helminths (parasitic worms; e.g., tapeworms, flukes) or ectoparasites (e.g., ticks, lice). Macroparasites also tend to be aggregated among hosts (Shaw et al., 1998). Explicitly considering the intensity of infection and the degree of aggregation is important in macroparasite models because the mortality of heavily infected hosts will result in disproportionate mortality in the parasite population, which in turn feeds back on host population health (Anderson and May, 1978). A less-recognized complication is that the degree of aggregation will change with any process that tends to select heavily infested hosts, such as parasite-induced host mortality, with subsequent impacts on parasite population dynamics. This additional complexity has hindered the development of spatially explicit models for macroparasite dynamics (Riley et al., 2015). Spatial effects have been *implicitly* included in macroparasite models via spatial patchiness in infection pressure (Cornell et al., 2004; May, 1978) or discrete geographic areas (Morgan et al., 2007), but models that *explicitly* track the movement of hosts and their parasites have been lacking (but see Milner and Zhao, 2008, who consider passive flow of parasites in a river system).

Explicitly spatial macroparasite models are needed to understand and predict how host

movement and parasitism might interact to affect wildlife health, which is especially important for migratory species. Existing models of parasite dynamics in migratory animals (e.g., Hall et al., 2014; Johns and Shaw, 2015; Hall et al., 2016; Morgan et al., 2007) do not consider how parasite burdens change dynamically over time and space or incorporate the dynamic processes occurring during movement that might influence parasite burdens, such as transmission and parasite-mediated migratory ability. These shortcomings not only limit our understanding for macroparasites, but ignore important aspects of host biology. Animals with high parasite burdens, for example, often show reduced migratory ability (Risely et al., 2017). Monarch butterflies infested with protozoan parasites are slower and fly shorter distances (Bradley and Altizer, 2005) and juvenile salmon infested with sea lice have reduced swimming performance (Nendick et al., 2011) and compromised schooling behavior (Krkošek et al., 2011). Parasite-mediated migratory ability may affect both the spatial distribution of hosts, reducing the distance migrated by parasitized individuals, and the spatial patterns in parasite burden, resulting in higher parasite burdens of stationary hosts left behind.

Here, we develop a new modelling framework for migratory-host and macroparasite population dynamics that considers dynamic changes in host abundance, parasite burden, and parasite aggregation. This extends previous host-macroparasite models (e.g., Anderson and May, 1978; Kretzschmar and Adler, 1993) to explicitly include spatial representation of a migration corridor. Parasite aggregation, as well as abundance, is allowed to change dynamically in space and time as a consequence of multiple interacting demographic, spatial, and epidemiological processes. First, we introduce the model and then we explore the model-predicted dynamics under a range of parameters. These simulation exercises provide new insights, such as the potential for parasite-mediated migratory stalling, and hint at the potential for broader application of the model in future studies.

Table 1: Abundance variables* in the migratory host-macroparasite model.

Symbol	Description
p_i	Abunance of stationary hosts with i parasites at (x,t)
$N = \sum_{i=0}^{\infty} p_i$	Abundance of the total stationary host population at (x,t)
$P = \sum_{i=0}^{\infty} ip_i$	Abundance of the total parasites on stationary hosts at (x,t)
$r_i = p_i/N$	Proportion of stationary hosts with i parasites
$m = P/N$	Mean parasite burden of stationary hosts
A	Variance-to-mean ratio (VMR) of parasites on stationary hosts
L	Density of infectious parasite larvae in the environment (section 2.2)

*Variables are all dependent on space and time (i.e., $p_i = p_i(x,t)$) but we have dropped the (x,t) for brevity. The variable for stationary hosts is shown, but the same variable exists for moving hosts, denoted by $\hat{}$.

2. Model

We develop a model that tracks changes in host abundance, parasite burden, and the aggregation of parasites along a one-dimensional migration corridor using a system of partial differential equations (PDEs). The model includes potential impacts of parasite burden on the migratory ability of hosts by dividing the host population into two categories: those that are moving at a constant speed and those that are stationary. We consider the rate at which hosts change from moving to stationary (i.e., stopping) to be a function of parasite burden. We also consider how the aggregation of parasites in the host population might change as the host population migrates (Adler and Kretzschmar, 1992; Kretzschmar and Adler, 1993). In the following section, we develop equations describing the spatiotemporal changes in host abundance, mean parasite burden, and the variance-to-mean ratio in the parasite distribution among hosts.

2.1. Birth, death, stopping, and starting

Following the approach of Anderson and May (1978) and Kretzschmar and Adler (1993), we begin with a system of differential equations that describe the number of hosts with i parasites, p_i. We extend the model of Kretzschmar and Adler (1993) to include a spatial

component, and distinguish moving and stationary hosts, where $p_i(x,t)$ is the number of stationary hosts with i parasites at location x and time t, and $\hat{p}_i(x,t)$ is the number of moving hosts at location x and time t. For all variables, we use $\hat{}$ to denote the moving population. Moving hosts stop at parasite-dependent rate γ_i and stationary hosts start moving at constant rate ω. Other parameters in the model do not directly depend on whether hosts are moving or stationary. Hosts are born parasite-free and stationary at rate β; we assume the host birth is independent of parasite burden, although this assumption could be relaxed in future models (e.g., Dobson and Hudson, 1992). Hosts die at natural rate μ, with additive parasite-induced mortality at per-parasite rate α (Anderson and May, 1978). Parasites attach at rate ϕ (see section 2.2), reproduce within the host at rate ρ, and die at rate σ. We assume that parasite demographic rates are density independent, except that the rate of parasite-induced host death depends on parasite burden. The basic model is described by four partial differential equations:

$$\frac{\partial p_0}{\partial t} = \beta \sum_{i=0}^{\infty}(p_i + \hat{p}_i) - (\mu + \phi)p_0 + \sigma p_1 + \gamma_0 \hat{p}_0 - \omega p_0 \tag{1}$$

$$\frac{\partial p_i}{\partial t} = -\left(\mu + \phi + i(\alpha + \sigma + \rho)\right) p_i + \sigma(i+1)p_{i+1} + \phi p_{i-1} + \rho(i-1)p_{i-1} + \gamma_i \hat{p}_i - \omega p_i \tag{2}$$

$$\frac{\partial \hat{p}_0}{\partial t} - c\frac{\partial \hat{p}_0}{\partial x} = -(\mu + \phi)\hat{p}_0 + \sigma \hat{p}_1 - \gamma_0 \hat{p}_0 + \omega p_0 \tag{3}$$

$$\frac{\partial \hat{p}_i}{\partial t} - c\frac{\partial \hat{p}_i}{\partial x} = -\left(\mu + \phi + i(\alpha + \sigma + \rho)\right) \hat{p}_i + \sigma(i+1)\hat{p}_{i+1} + \phi \hat{p}_{i-1} + \rho(i-1)\hat{p}_{i-1} - \gamma_i \hat{p}_i + \omega p_i \tag{4}$$

for all $i \geq 1$. Descriptions of the variables and parameters are given in Tables 1 and 2, respectively. In Appendix A, we show that the solution to equations (1-4) and equation (5) are bounded, positive, and unique for all $t \geq 0$, $x \in \Omega$, and $i \in \{1, \ldots, I\}$, where I is some number of parasites larger than the carrying capacity of hosts, provided $p_i(0,x)$, $\hat{p}_i(0,x)$,

Table 2: Parameters in the migratory host-macroparasite model.

Symbol	Description	Baseline value	Units
β	Host birth	0	yr^{-1}
μ	Natural host mortality	0	yr^{-1}
ϕ	Parasite attachment	see section 2.2	yr^{-1}
α	Parasite-induced host mortality	0.1	$\text{parasite}^{-1}\ \text{yr}^{-1}$
ρ	Within-host parasite reproduction	0	$\text{parasite}^{-1}\ \text{yr}^{-1}$
σ	Within-host parasite mortality	5	$\text{parasite}^{-1}\ \text{yr}^{-1}$
κ	Production of free-living parasites	1	yr^{-1}
λ	Infection probability	0.01	
μ_L	Mortality of free-living parasites	5	yr^{-1}
c	Migration speed	10 000	km yr^{-1}
γ	Stopping rate	1	yr^{-1}
θ	Per-parasite increase in stopping	0	$\text{parasite}^{-1}\ \text{yr}^{-1}$
ω	Starting rate	1	yr^{-1}

and $L(0,x)$ are non-negative, continuously differentiable, and integral in $\mathbb{R}$. Although I in the system of equations (1-4) above is infinite (as parasite attachment can always lead to hosts with more parasites), considering I finite or $I=+\infty$ are equivalent if the distribution of parasites among hosts has finite moments (Appendix A.4).

2.2. Attachment rate

The per-host attachment of parasites takes place at rate ϕ, in proportion to the number of infectious parasites at (x,t). We derive a formula for ϕ by considering a transmission stage of larval parasites, $L(x,t)$, that are free-living, such as eggs, spores, or cysts. These larval parasites exist outside of the (primary) host and are assumed to be stationary relative to the distances moved by the migratory host population. The dynamics of the larval parasites are described by:

$$\frac{\partial L}{\partial t} = \kappa(P+\hat{P}) - \mu_L L - \lambda L(N+\hat{N}), \tag{5}$$

where κ is the within-host rate of production of larvae by attached parasites, P and $\hat{P}$ are the total densities of attached parasites on stationary and moving hosts, respectively, μ_L is the mortality rate of larval parasites, λ is the infection rate, and N and $\hat{N}$ are the densities of stationary and moving hosts, respectively (see section 2.4). The per-host rate of attachment is therefore $\phi = \lambda L$.

In cases where the development time of eggs, cysts, or spores is short, it may be justifiable to assume that the dynamics of parasite production and attachment occur on much faster timescales than the lifespans of hosts and parasites (Anderson and May, 1978). We refer to this as direct transmission because the time that parasite larvae spend in the environment is assumed to be negligible. In the case of direct transmission, we can assume that equation (5) is at equilibrium or quasi-equilibrium:

$$L^* = \frac{\kappa(P + \hat{P})}{\mu_L + \lambda(N + \hat{N})}, \tag{6}$$

in which case the attachment rate becomes:

$$\phi = \lambda L^* = \frac{\kappa(P + \hat{P})}{\mu_L/\lambda + N + \hat{N}}. \tag{7}$$

The timescale assumption eliminates the need to track the dynamics of L explicitly. However, we have chosen to model L explicitly because the infection rate of moving hosts is sensitive to the difference between infection and mortality rates of free-living larvae, allowing for dynamics like migratory escape.

2.3. Movement status

Hosts are classified as either stationary or moving. Moving hosts migrate at a constant speed, c, regardless of the number of parasites they harbour, but hosts stop moving at parasite-dependent rate γ_i and stationary hosts start moving at constant rate ω. We assume that the stopping rate increases linearly with the number of parasites in or on a host: $\gamma_i =$

$\gamma + \theta i$, where θ is the per-parasite increase in the stopping rate. Although a saturating stopping rate may be more realistic, once γ_i becomes much greater than ω, most hosts will be stationary and the rate of stopping becomes biologically irrelevant. We assume for our analysis that the rate of starting does not depend on parasites, but depending on the system of interest, ω could also be a function of parasite burden. For an initial exploration of the model's behavior, this seems to be a biologically reasonable assumption because if an individual's ability to migrate is adversely affected by parasites, they may still experience the drive to complete the migration, but as parasite burden increases their progress will be hindered as they make increasingly frequent stops.

2.4. Equations for the total population size

We can write equations for the total host population (N and $\hat{N}$) and total parasite population (P and $\hat{P}$) at (x, t) by summing equations for p_i and $\hat{p}_i$ over all possible numbers of parasites (Table 1). The aggregate equations are:

$$\frac{\partial N}{\partial t} = \beta(N + \hat{N}) - (\mu + \omega)N - \alpha P + \gamma\hat{N} + \theta\hat{P} \tag{8}$$

$$\frac{\partial P}{\partial t} = \rho P - (\mu + \omega + \sigma)P + \phi N + \gamma\hat{P} - \alpha N \sum_{i=0}^{\infty} i^2 r_i + \theta\hat{N} \sum_{i=0}^{\infty} i^2 \hat{r}_i \tag{9}$$

$$\frac{\partial \hat{N}}{\partial t} - c\frac{\partial \hat{N}}{\partial x} = -(\mu + \gamma)\hat{N} - (\alpha + \theta)\hat{P} + \omega N \tag{10}$$

$$\frac{\partial \hat{P}}{\partial t} - c\frac{\partial \hat{P}}{\partial x} = \rho\hat{P} - (\mu + \sigma + \gamma)\hat{P} + \phi\hat{N} + \omega P - \hat{N}(\alpha + \theta) \sum_{i=0}^{\infty} i^2 \hat{r}_i, \tag{11}$$

where r_i and $\hat{r}_i$ are the proportion of stationary and moving hosts, respectively, harbouring i parasites (Table 2). The original model in equations (1-4) cannot be completely described by the above equations because the summations over r_i require information on the distribution of parasites among hosts.

2.5. Mean parasite burden and the variance-to-mean ratio

The mean parasite burden is the expected number of parasites that a host would have. To provide a more biologically intuitive measure of the infection level, we can rewrite equations (8-11) as a function of the mean parasite burdens per host, m and $\hat{m}$. The variables m and $\hat{m}$ are well defined because N and $\hat{N}$ remain positive for all t and x (Appendix A). Using the chain rule:

$$\frac{\partial m}{\partial t} = \frac{1}{N}\frac{\partial P}{\partial t} - \frac{m}{N}\frac{\partial N}{\partial t}. \tag{12}$$

We also introduce the variance-to-mean ratio (VMR), A, which describes the aggregation of parasites among hosts. We can write the summations in equations (8-11) in terms of the VMR:

$$\sum_{i=0}^{\infty} i^2 r_i = \text{variance} + m^2 = m(A + m). \tag{13}$$

Calculating the change in mean number of parasites per host using equation (13) we arrive at:

$$\frac{\partial N}{\partial t} = \beta(N + \hat{N}) - (\mu + \omega + \alpha m)N + (\gamma + \theta\hat{m})\hat{N} \tag{14}$$

$$\frac{\partial m}{\partial t} = \rho m + \phi - m\left(\sigma + \alpha A + \beta\left(\frac{N + \hat{N}}{N}\right)\right) + \frac{\hat{N}}{N}\left(\gamma(\hat{m} - m) + \theta\hat{m}(\hat{A} + \hat{m} - m)\right) \tag{15}$$

$$\frac{\partial \hat{N}}{\partial t} - c\frac{\partial \hat{N}}{\partial x} = -\Big(\mu + \gamma + (\alpha + \theta)\hat{m}\Big)\hat{N} + \omega N \tag{16}$$

$$\frac{\partial \hat{m}}{\partial t} - c\frac{\partial \hat{m}}{\partial x} = \rho\hat{m} + \phi - \hat{m}\Big(\sigma + (\alpha + \theta)\hat{A}\Big) + \frac{N}{\hat{N}}\omega(m - \hat{m}). \tag{17}$$

As previously mentioned, macroparasites are often aggregated among hosts with a distribution that is well described by the negative binomial (Shaw et al., 1998). Thus, we proceed by assuming that parasites are distributed according to the negative binomial with mean

parasite burden m and overdispersion parameter k. The VMR is related to the overdispersion parameter by $k = m/(A-1)$. Although many macroparasite models assume that k is constant (and therefore the VMR changes predictably with the mean) (e.g., Anderson and May, 1978; May, 1978; Krkošek et al., 2011), we do not make this simplifying assumption because we expect that the aggregation of parasites among hosts will change in space and time with parasite-mediated migratory behaviour and parasite-induced host mortality. In the following section, we follow the approach of Kretzschmar and Adler (1993) and derive the equation for the VMR as an additional dynamic variable.

2.6. Variance-to-mean ratio as a dynamic variable

We derived equations for the change in the VMR of parasites on stationary and moving hosts, A and $\hat{A}$, respectively, following the approach of Kretzschmar and Adler (1993). The derivation of the VMR equations, and the general form that can be applied for parasite distributions other than the negative binomial, can be found in Appendix B. If we proceed with the assumption that parasites are distributed according to the negative binomial, we can write the equations for the dynamic VMR as:

$$\begin{aligned}\frac{\partial A}{\partial t} = \beta m\left(\frac{N+\hat{N}}{N}\right) + 2\rho + (1-A)\left(\frac{\phi}{m} - \rho + \sigma + A\alpha\right) \\ + \frac{\hat{N}\hat{m}}{Nm}\Big[\theta\Big(\hat{A}(3\hat{m} + 2\hat{A} - 1 - A - 2m) + (\hat{m}-m)^2 - A\hat{m}\Big) \\ + \gamma\Big(\hat{m} + \hat{A} - A - 2m + \frac{m^2}{\hat{m}}\Big)\Big] \qquad (18)\end{aligned}$$

$$\begin{aligned}\frac{\partial \hat{A}}{\partial t} - c\frac{\partial \hat{A}}{\partial x} =& 2\rho + (1-\hat{A})\left(\frac{\phi}{\hat{m}} - \rho + \sigma + \hat{A}(\alpha+\theta)\right) \\ &+ \frac{Nm}{\hat{N}\hat{m}}\omega\left(m + A - \hat{A} - 2\hat{m} + \frac{\hat{m}^2}{m}\right) \qquad (19)\end{aligned}$$

The complete system describing the spatial and temporal dynamics of hosts and parasites under the negative binomial assumption is described by equations (14-17) and (18-19).

3. Simulations and results

In this section, we illustrate how migration can affect parasite burden and the importance of including a dynamically changing VMR using simulations of the host-macroparasite model introduced in section 2. In its basic form, the model captures the spatiotemporal disease dynamics along the migration corridor but does not consider the full annual migration cycle, including overwintering and breeding. However, in section 3.4 we also illustrate how the model can be extended to consider breeding and overwintering seasons when a host population is not migrating.

3.1. Simulation methods

We simulated the model over a discrete space-time grid using a numerical scheme that, at each time step, split the problem between two different processes: (1) spatial dynamics of moving populations and (2) temporal dynamics of birth, mortality, and switching movement status. This approach is known as operator splitting in the numerical solution of advection-diffusion-reaction equations (Hundsdorfer and Verwer, 2013). We considered a migration corridor that was long enough to accommodate migrants who moved for the entire simulation (migration season), which eliminated the effect of boundary conditions. An alternative approach that may be more appropriate if the end of the migration occurred at a certain point in space would be to consider an absorbing boundary. For details of our numerical methods, see Appendix C.

The model we have described is general, and different parameterizations make it adaptable to a variety of life-histories of both the parasite and host. For our initial exploration of the dynamics, we considered a theoretical population migrating 2000 km along a one-dimensional migration corridor, with a spatial grid consisting of steps $\Delta x = 1$ km in length. First, we consider the migratory season only when hosts have left their breeding grounds and therefore host reproduction is $\beta = 0$ yr^{-1}. In section 3.4, we consider $\beta > 0$ during a breeding season. Other parameters were varied from their baseline values (Table 2) in

sensitivity analyses exploring their effect on the dynamics, with details given in the relevant sections below. The migration period lasted 0.2 yr (or 73 days), simulated using a time step of $\Delta t = 0.0001$ yr.

We initiated all simulations with a host population that had a peak abundance of 1000 individuals at the start of the migration (arbitrarily set at 130 km) and a Gaussian spatial distribution with a standard deviation of 30 km. We added one individual to both the initial moving and stationary host populations to ensure the problem was well posed; we required that N and P be positive in order to define m and A (Appendix A) and to avoid numerical issues when host abundance was zero due to the ratios in equations (18-19). This meant that host abundance was never exactly zero in our simulations. We assumed an initial parasite burden of $m(x,0) = \hat{m}(x,0) = 5$ parasites per stationary and moving host with overdispersion of $k = 0.8$, giving a VMR of $A(x,0) = \hat{A}(x,0) = 7.25$. The initial density of free-living parasites was $L(x,0) = 1$ km^{-1}.

3.2. Parasite burden of moving and stationary populations

We contrasted the parasite dynamics of non-migratory and migratory host populations with the production of free-living parasites ranging from $\kappa = 0$ to $\kappa = 10$ parasite^{-1} yr^{-1} and the within-host reproduction ranging from $\rho = 0$ to $\rho = 10$ parasite^{-1} yr^{-1}. We hypothesized that increases in ρ would affect parasite burdens of stationary and migrating hosts in a similar way because within-host reproduction of parasites would track the movement of migratory hosts. In contrast, increases in κ would emphasize any differences in parasite dynamics between stationary and migrating hosts because migratory hosts will move away from areas where free-living parasites accumulate.

For these simulations, we set $\gamma = \omega = 0$ and $\theta = 0$ so that hosts did not switch between stationary and moving. The initial non-migratory host population was entirely stationary and remained so throughout the simulation. The initial migratory host population was entirely moving and therefore migrated at the constant speed c for the duration of the simulation. We report the host abundance, parasite burden, VMR, and density of free-living

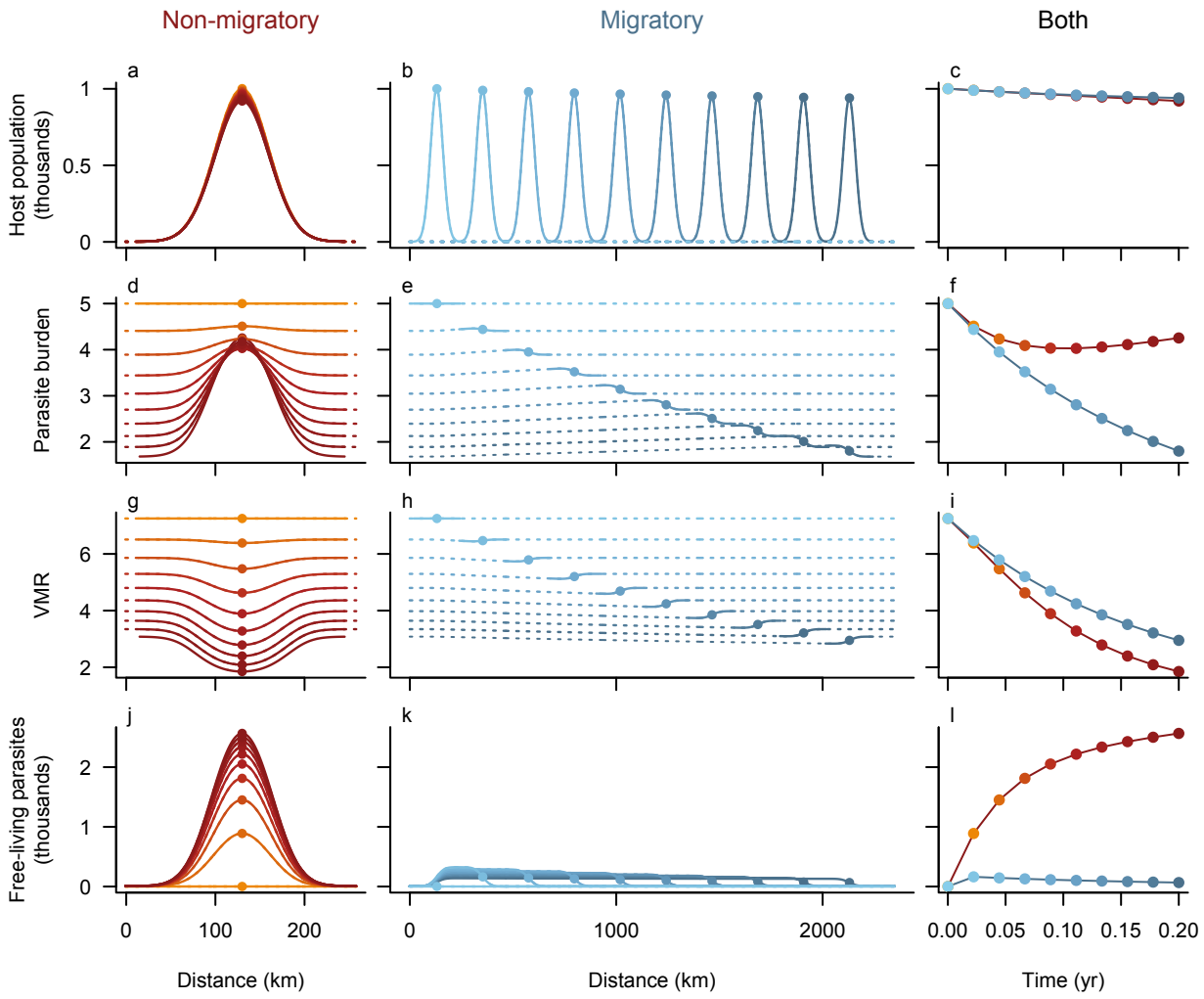

Figure 1: Host abundance for a non-migratory population (a; red) and a migratory host population that migrates 2000 km (b; blue) from $t = 0$ (orange/light blue) to $t = 0.2$ yr (dark red/blue). Parasite burdens declined in both cases but were much lower at the end of the migration season for migratory populations (e) than non-migratory populations (d), due to migratory escape from the buildup of free-living parasites (j,k). Dotted lines correspond to regions in space where host abundance was less than one individual. The change over time in variables at peak host abundance is shown on the right, emphasizing differences between migratory (red) and non-migratory (blue). Parameters for the simulation are given in Table 2, with the exception of $\omega = 0$, $\gamma = 0$, $\rho = 0$, and $\kappa = 10$. See `https://rawgit.com/sjpeacock/Migration_model/master/MigVsStat.html` for an animated version.

parasites after 0.2 yr for the non-migratory and migratory populations (Fig. 1). These variables correspond to the stationary and moving populations for the non-migratory and migratory simulations, respectively, because hosts were not allowed to switch movement status in these simulations.

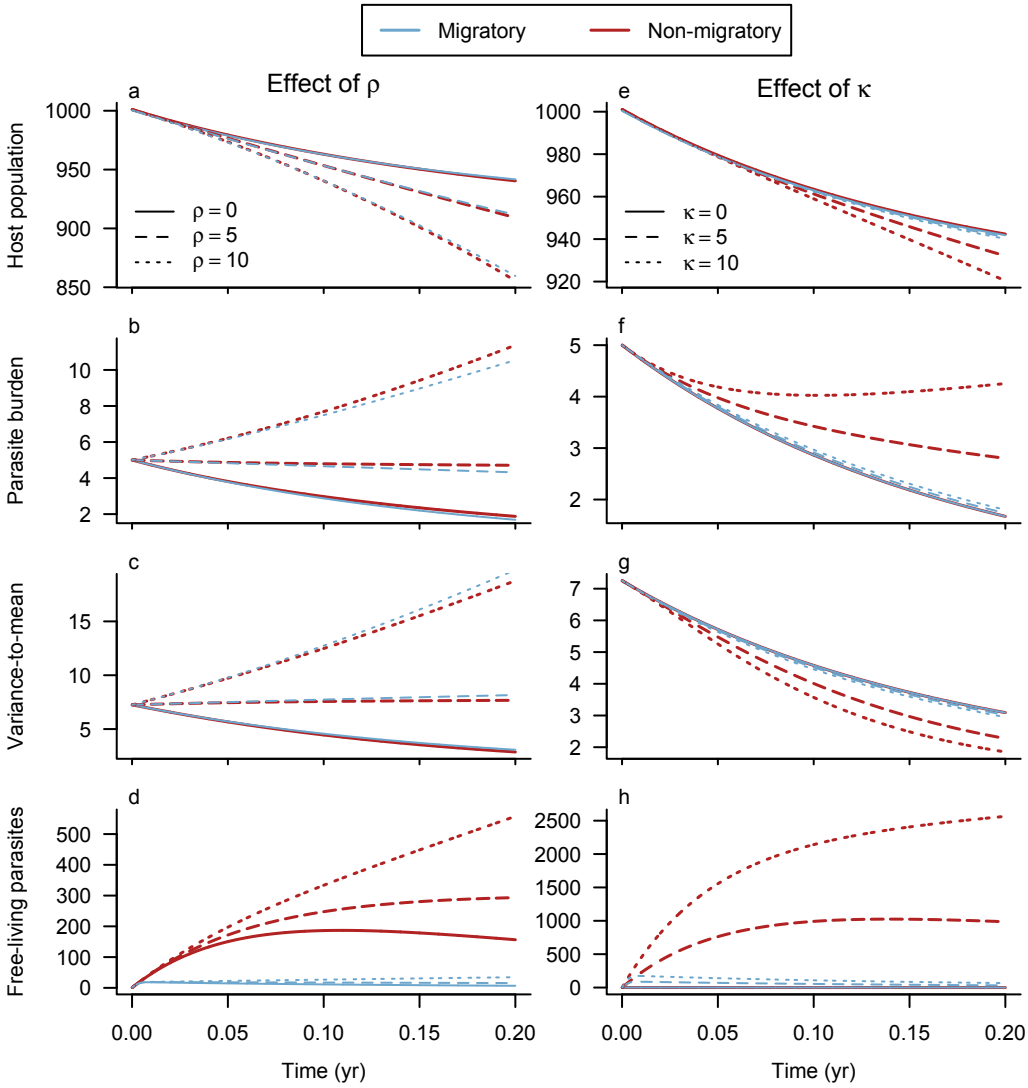

Figure 2: The host population (a,e), parasite burden (b,f), VMR (c,g), and density of free-living parasites over time for increasing within-host parasite reproduction (ρ, left) and production of free-living parasites (κ, right). As for the right-hand column of Fig. 1, dark red lines correspond the non-migratory populations at the initial location $x_0 = 130$ km and the lighter blue lines correspond to the migrating populations at the location of peak host abundance (i.e., $x(t) = x_0 + ct$).

The effect of increasing within-host parasite production had similar effects for non-migratory and migratory populations, as we predicted. As ρ increased, host populations

declined more rapidly (Fig. 2a), parasite burdens increased more rapidly (Fig. 2b), and parasites were more aggregated among hosts (Fig. 2c). The build-up of free-living parasites at the location of the non-migratory host population was higher (Fig. 2d) and resulted in slightly higher parasite burdens on non-migratory hosts than on migratory hosts.

Increases in κ also led to lower host densities, but the effect was much larger for non-migratory hosts (Fig. 2e). Parasite burden was higher for non-migratory hosts than migratory hosts when $\kappa > 0$ (Fig. 1, Fig. 2f). While increasing ρ resulted in a higher VMR (Fig. 2c), increasing κ had the opposite effect (Fig. 2g); parasites were less aggregated because infection by free-living parasites occurred at random, evening out the parasite distribution among hosts. The simultaneous decline in host population (Fig. 2e), parasite burden (Fig. 2f), and VMR (Fig. 2g) for both non-migratory and migratory populations suggest that the most heavily infected hosts are suffering parasite-induced mortality. The VMR declined more rapidly for non-migratory hosts than migratory hosts as κ increased (Fig. 2g) due to parasite-induced mortality culling heavily infected individuals. For non-migratory populations, new infections may have been more important in lowering the VMR as the exposure to free-living parasites was much higher for non-migratory hosts (Fig. 2h).

3.3. Effect of dynamic variance-to-mean ratio

Kretzschmar and Adler (1993) were the first to consider modelling the VMR as an additional dynamic variable. They found that hosts and parasites coexist at a stable equilibrium only if the VMR increases with increasing mean of the parasite distribution, due to the associated increase in per capita parasite death with higher parasite loads. However, they also found that in cases with very strong aggregation, parasites may be unable to effectively control the host population and the system is unstable. Therefore, to say something about stability, it is necessary to include the VMR as a dynamic variable whenever parasite burden affects host survival and therefore parasite survival. But what of our migratory model, where it is the transient dynamics during a migration season that are of interest? How does a dynamic VMR affect parasite burdens and host densities compared to simpler models?

To answer this question, we compared simulations using three variants of the model: (1) the Poisson model, assuming a Poisson distribution of parasites among hosts where the variance was always equal to the mean (i.e., $A(x,t) = \hat{A}(x,t) = 1$ and $k \to \infty$), (2) the constant aggregation model, assuming a negative binomial distribution of parasites among hosts with a constant aggregation parameter of $k = 0.8$ such that $A(x,t) = m(x,t)/k + 1$ and $\hat{A}(x,t) = \hat{m}(x,t)/k + 1$, and (3) the dynamic VMR model given by equations (18-19). In a spatial context, we were most interested in how these models compared when parasites had a strong influence on the rate of host stopping. Therefore, we compared simulations under baseline parameter values (Table 2) with the exception of the per-parasite increase in stopping which we set at $\theta = 10$.

For each variant of the model, the parasite burden was always higher on stationary hosts than on moving hosts due to the tendency for infected hosts to have higher rates of stopping (Fig. 3b). This parasite-induced migratory stalling also led to a relatively high abundance of stationary hosts at the start of the migration, where parasite burdens were highest, and a long-tail that extended behind the moving population as hosts stopped along the migration route.

The Poisson distribution led to the lowest host abundance (Fig. 3a) and the highest mean parasite burden (Fig. 3b) for the moving population. Under the Poisson model, parasites were more evenly distributed among hosts and so the prevalence of infection was higher for a given mean parasite burden. Thus, a larger proportion of the host population experienced an increase in stopping rates, leading to fewer moving hosts. Further, parasite-induced stopping was less effective at reducing the mean parasite burden of moving hosts, leading to higher mean parasite burdens among moving hosts.

The constant aggregation and dynamic VMR models predicted very similar host densities along the migration (Fig. 3a), but there were slight differences in the parasite burdens (Fig. 3b). As might be expected when migratory ability depends on parasite load, the dynamic VMR model predicted higher parasite burdens at the tailing edge of the moving population,

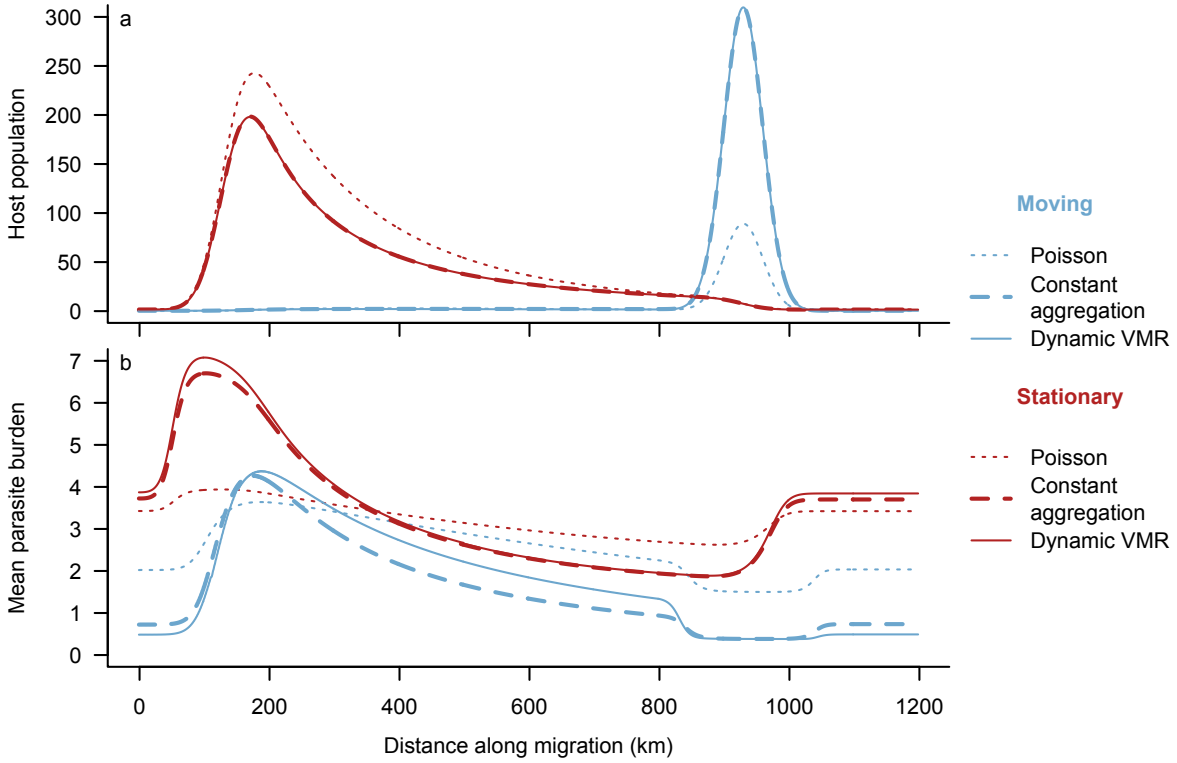

Figure 3: The spatial distribution of moving and stationary hosts (a; $\hat{N}(x,t)$ and $N(x,t)$, respectively) and their respective mean parasite burdens (b; $\hat{m}(x,t)$ and $m(x,t)$), part-way through a migration at $t = 0.08$ yr (approx. 30 days). The full model given by equations (18-19) was simulated but the solutions for VMR and the density of infectious parasite larvae in the environment are not shown. The per-parasite increase in the rate of stopping was high ($\theta = 10$), resulting in much of the host population being left behind and a lower parasite burden on those hosts that continue to migrate. All other parameters were at their baseline values (Table 2).

and lower parasite burden at the centre and leading edge of the moving population.

3.4. Annual dynamics

Thus far, we have focused on migration and ignored host reproduction and natural mortality. In many systems, hosts will migrate between breeding and overwintering grounds and parameters in the model may differ among these seasons. To illustrate how the model can be used to understand host-parasite dynamics over an annual cycle, we combined simulations using different parameters for each of four seasons within a year: breeding, fall migration, overwintering, and spring migration. During the breeding and overwintering seasons, we assumed that all hosts were stationary with $\gamma = \omega = 0$ so that no hosts switched to migrat-

ing. During the breeding season, hosts reproduced at rate $\beta = 2.5$ yr^{-1}, and for all other seasons we set $\beta = 0$ yr^{-1}. At the beginning of the migration seasons, all hosts switched from stationary to moving at speed $c = 10000$ km yr^{-1}. At the end of migration seasons, moving hosts and their parasites switched back to stationary wherever they were when the migration season ended, and remained there for the following breeding or overwintering season. We ignored stopping, starting, and migratory stalling, keeping $\gamma = \omega = 0$ and $\theta = 0$ for simplicity (this assumption could be relaxed in future analyses). Other parameters were set at their baseline values (Table 2) except for the mortality of free-living parasites, which we varied from $\mu_L = 0.5$ to the baseline value of $\mu_L = 5$ and host mortality which was highest during migration ($\mu_L = 0.1$) and lowest during the breeding season ($\mu = 0.05$) with overwintering intermediate between those two ($\mu_L = 0.08$).

We report the host abundance and parasite burden over a 100-year simulation at the location of peak host abundance in space. The peak host abundance was centred at the breeding grounds during the breeding season (i.e., 130 km along the spatial corridor), at the overwintering grounds during the overwintering season (i.e., 2130 km), and moved in between those two locations during the migration seasons. At baseline parameter values (Table 2), we observed cyclic dynamics in host abundance and parasite burden with a period of ≈ 8 years (Fig. 4a). Parasite burden tended to lag a year or so behind host abundance, which has also been observed in previous host-macroparasite models that display cyclic dynamics (Dobson and Hudson, 1992). Within a given year, we saw an increase in host abundance during the breeding season and a decline in host abundance throughout the rest of the year due to natural and parasite-induced mortality (Fig. 4b). During the first decade of the simulations, the parasite burden increased during the breeding season, declined during migration, and increased again during overwintering. However, over the longer term, this annual pattern did not hold (Fig. 4b), perhaps due to the buildup of free-living parasites along the migration route eroding some benefit of migratory escape.

To understand the effect of migration on multi-year host-parasite dynamics, we compared

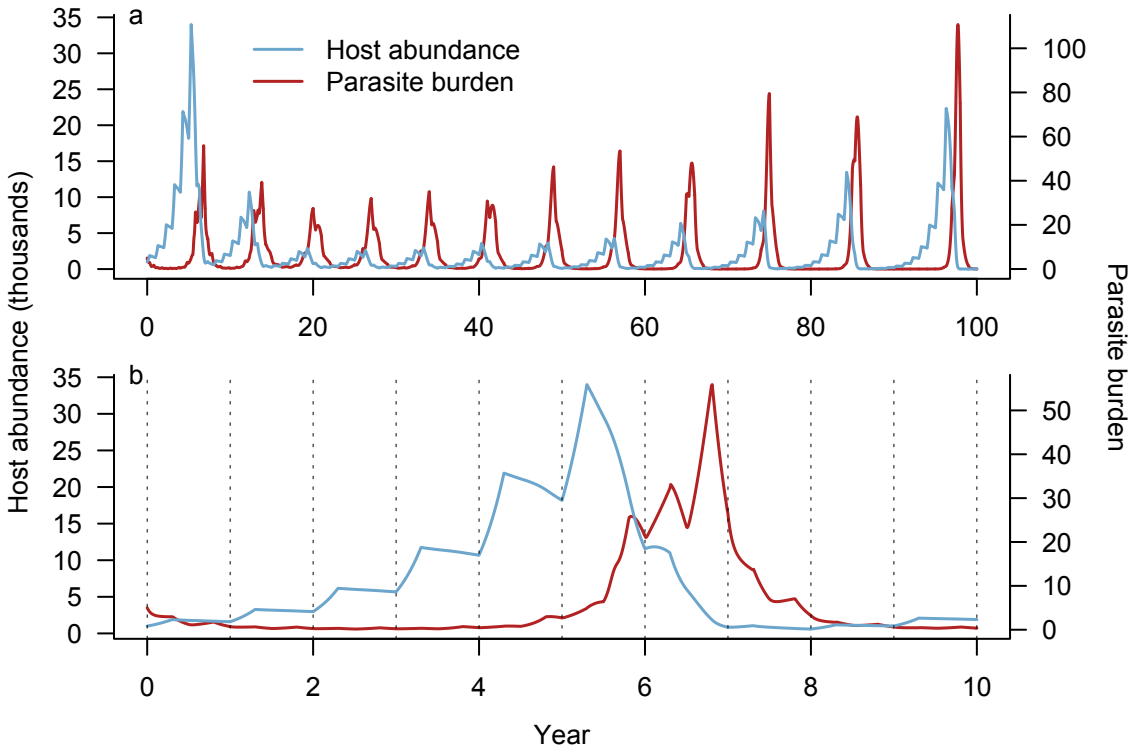

Figure 4: The host abundance (light blue; left axis) and parasite burden (dark red; right axis) over a 100-year simulation including breeding, migration, and overwintering seasons. Over long time-scales, the dynamics are cyclic with a period of ~ 8 years (a). Zooming in on the first decade (b), we also observe fluctuations within a year, with host abundance peaking after the breeding season and parasite burden rising during breeding and overwintering, and declining during migrations. Parameters were at baseline values (Table 2) except host birth and natural host death which changed with season (see main text for details).

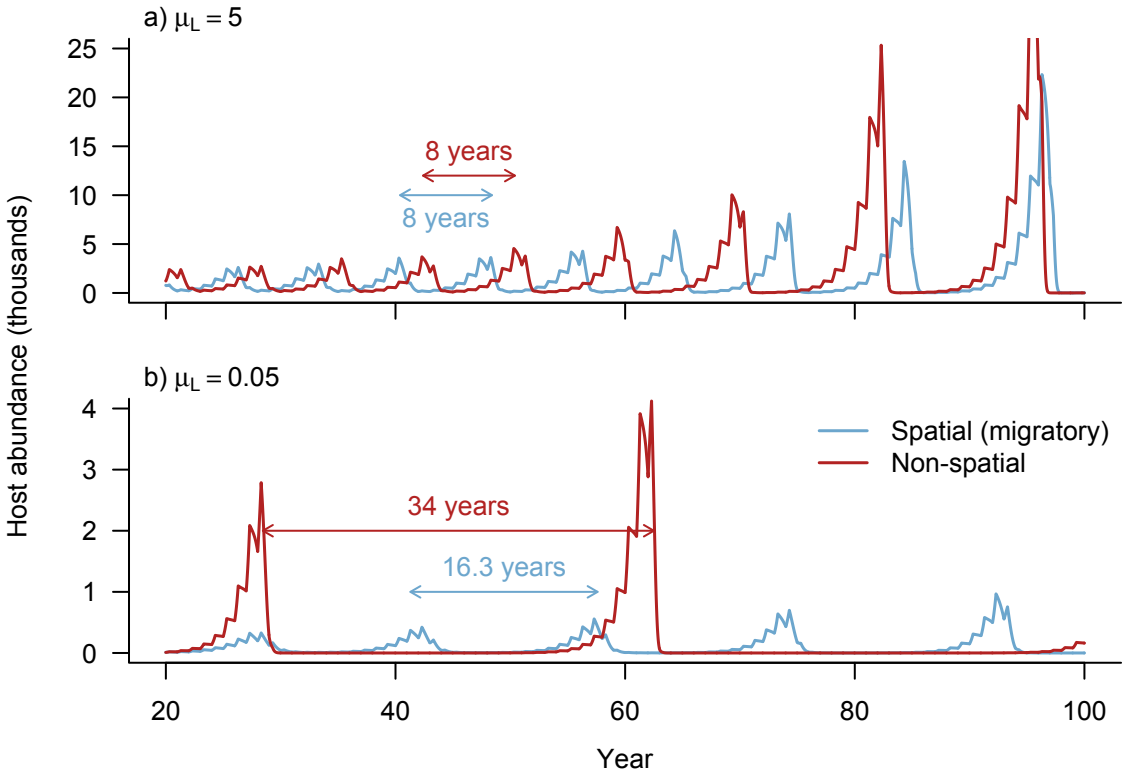

Figure 5: The host abundance over the last 80 years of a 100-year simulation using a model for a migratory population that experienced breeding, migration, and overwintering seasons (light blue lines) and a non-spatial model where all parameters were the same but hosts did not migrate (dark red lines). The period of cycles in the non-spatial model were similar when the mortality of free-living parasites was high ($\mu_L = 5$, b), but differed when mortality of free-living parasites was low ($\mu_L = 5$, d).

the dynamics of our spatially explicit migration model to the dynamics of the non-spatial model developed by Kretzschmar and Adler (1993) that was otherwise the same (i.e., included dynamic VMR). For the non-spatial simulations, we still assumed four seasons within the year but the "migratory" seasons did not include the movement of hosts. This altered the dynamics in that the density of free-living parasites that hosts encountered only changed due to host and parasite dynamics but not due to host movement away from larval patches as for the spatial model. We used the same parameterization as for spatial model in order to isolate the effect of adding a spatial component on host-parasite dynamics.

Predictions from the non-spatial model showed similar qualitative behaviour as our spatial model when the mortality of free-living parasites was high; populations underwent cycles with approximately the same amplitude and period whether or not spatially explicit migration was included (Fig. 5a). When the mortality of free-living parasites was low, both models predicted lower host abundances (Fig. 5b), likely due to a higher abundance of free-living parasites in the environment regulating host populations. However, our spatial model predicted lower and more frequent peaks in host abundance than the non-spatial model (Fig. 5b). The frequency of cycles was more similar to the high μ_L scenario than for the non-spatial model, likely because the migration away from infection hotspots mitigated the effect of low free-living parasite mortality. Conversely, in the non-spatial model, hosts could not move away from high densities of free-living parasites that accumulate when the mortality of free-living parasites is low, and so the dynamics were quite different under low μ_L than under high μ_L.

4. Discussion

Animal migrations may have profound implications for parasite dynamics in wildlife by spreading parasites to new areas, allowing hosts to escape infection hotspots, or culling infected individuals from host populations (Altizer et al., 2011). These mechanisms may influence parasite burdens of migratory hosts in opposing ways, making it difficult to under-

stand the net effect of migration on animal health. We recognized a need for a modelling framework that could incorporate host migration and macroparasite dynamics to predict the conditions under which we might expect, for example, migratory escape from parasites. In this paper, we developed such a framework and showed how it builds upon previous models of host-parasite dynamics by explicitly accounting for parasite burden and aggregation, including spatial dynamics, and allowing the distribution of parasites among hosts to change dynamically in space and time.

Migration can be energetically taxing, and the extra cost of infection may compromise a host's ability to keep up with the herd (Risely et al., 2017). Our analysis revealed a phenomenon we have termed parasite-induced migratory stalling, whereby parasite-impacts on migratory ability can lead to positive feedbacks in parasite transmission that may result in the host population halting their migration. Our model is the first to exhibit this behavior because it includes two key features that previous models (e.g., Hall et al., 2014; Johns and Shaw, 2015) were lacking: transmission dynamics during migration and spatiotemporal dynamics of the parasite burden of hosts. These features allowed us to explore how parasite-mediated increases in the rate that hosts stop moving affect migratory ability and parasite burdens. When the rate of stopping increased with parasite burden, we found that hosts tended to accumulate in the stationary category. In the case of parasites that are environmentally transmitted, moving hosts can escape infection hotspots while stationary hosts experience higher infection pressure. We also observed spatial structure in the parasite burden even within the moving host population; hosts at the leading edge of the migration tended to have lower parasite burdens than hosts at the tailing edge, while stationary hosts had even higher parasite burdens. Our model simulations were not specific to any biological system, but specific parameterizations could be adopted to understand, for example, the potential for migratory stalling of birds at stopover sites, which tend to be infection hotspots, or the risk of migratory stalling for wildlife in contact with domesticated animals that can act as reservoir hosts.

Our model predictions are consistent with several empirical studies of parasite burdens in migratory wildlife. In species that show partial migration, where only certain populations display migratory behaviour, sedentary populations often have higher parasite burdens across taxa. For example, in Canada, migratory elk are less likely to be infected with the trematode *Fascioloides magna* than resident populations (Pruvot et al., 2016). Similarly, the migration of red deer in Norway is associated with lower tick abundance (Qviller et al., 2013). The loss of migratory behaviour in certain populations of monarch butterflies in the USA has led to higher prevalence of protozoan parasites than in migratory conspecifics (Satterfield et al., 2015). Further studies have shown a negative relationship between the distance migrated and parasite prevalence (e.g., Bartel et al., 2011). Globally, animal migrations are under increasing pressure from anthropogenic environmental change with observed declines in migratory behaviour (Wilcove and Wikelski, 2008). Quantitative models such as ours allow scientists to predict the potential consequences for animal health.

Although limited in scope, the annual simulations illustrated how our model could be used to understand seasonal effects of migration and host breeding on parasite dynamics, and the long-term implications of seasonal or climatic changes in parameters such as the mortality of free-living parasites. We found that host and parasite populations tended to cycle on long timescales, but the exact period of oscillations depended on the mortality of free-living parasites. Red grouse have classically illustrated such population cycles and experimental studies have suggested that parasites may be the cause of these cycles (Hudson and Greenman, 1998), although other factors are likely also at play (Redpath et al., 2006). Many wildlife populations display such cycles, including migratory species such as caribou (Ferguson et al., 1998), leaving it open for future work to examine possible links with parasitism. If parasites are contributing to population cycles, then our model simulations suggest that changes to the mortality of free-living parasites due to, for example, climate change (Dobson et al., 2015), may have important consequences for the period of host population cycles. The presence of migratory behaviour tended to mitigate changes to

population cycles that resulted from reduced parasite mortality, suggesting that migratory species might be more resilient to changes in parasite survival. Alternatively, higher survival of free-living parasites combined with the loss of migratory behavior associated with global anthropogenic change (Wilcove and Wikelski, 2008) could lead to dramatic changes in host population cycles.

One important aspect of migration that is missing from our model is the collective behavior of migratory animals. We assume that an individual's movement depends on parasite burden but is independent of what other animals in the herd, school, or flock are doing. In reality, many animal groups move as a cohesive unit to avoid predation and increase foraging efficiency (Alexander, 1974). Thus, a single individual with a high parasite burden may be left behind, but perhaps healthy individuals would hang back if the prevalence of parasitism in the herd was high. This kind of collective behavior may exacerbate the effect of migratory stalling that we have described. Models with simple rules for attraction, repulsion, and orientation among neighbours in a herd can reproduce the seemingly complex group dynamics observed in nature (e.g., Couzin et al., 2002; Eftimie et al., 2007). Incorporating the effects of parasites into these simple rules may provide insight into how collective dynamics would affect the inferences we have made, and is an area for future research.

The model we have presented is a general framework for host-macroparasite dynamics along a spatial domain, such as a migration corridor. Because of its generality, it can be adapted to answer a number of important questions facing wildlife disease ecology. What are the conditions under which we might expect migratory escape, migratory culling, or migratory stalling? How might the effect of rising temperatures on developmental rates of parasites and/or migration timing of hosts affect the health of migrating animals? More than just changing parameters, the structure of the model can be adapted in various ways; for example, to examine how reservoir hosts, such as domestic animals, influence parasite dynamics of sympatric migratory wildlife. We have provided the basic framework for these and other future studies that will shed light on how parasites might affect wildlife populations

in a changing world.

5. Acknowledgements

We thank Martin Krkošek for motivating discussions. The authors gratefully acknowledge funding from an NSERC Vanier Scholarship and Postdoctoral Fellowship to SJP, NSERC Discovery Grants to MAL and PKM, a Canada Research Chair to MAL, and a postdoctoral fellowship from the Pacific Institute for Mathematical Sciences to JB.

6. Literature cited

Adler, F.R., Kretzschmar, M., 1992. Aggregation and stability in parasite-host models. Parasitology 104, 199–205. doi:10.1017/S0031182000061631.

Alexander, R.D., 1974. The Evolution of Social Behavior. Annual Review of Ecology and Systematics 5, 325–383. doi:10.1146/annurev.es.05.110174.001545.

Altizer, S., Bartel, R., Han, B.A., 2011. Animal Migration and Infectious Disease Risk. Science 331 (6015), 296–302. doi:10.1126/science.1194694.

Anderson, R.M., May, R.M., 1978. Regulation and stability of host-parasite population interactions: I. Regulatory processes. Journal of Animal Ecology 47 (1), 219–247.

Anderson, R.M., May, R.M., 1979. Population biology of infectious diseases: Part I. Nature 280 (5721), 361–367. doi:10.1038/280361a0.

Bartel, R.A., Oberhauser, K.S., De Roode, J.C., Altizer, S.M., 2011. Monarch butterfly migration and parasite transmission in eastern North America. Ecology 92 (2), 342–351. doi:10.1890/10-0489.1.

Bradley, C.A., Altizer, S., 2005. Parasites hinder monarch butterfly flight: implications for disease spread in migratory hosts. Ecology Letters 8, 290–300. doi:10.1111/j.1461-0248.2005.00722.x.

478 Cornell, S.J., Isham, V.S., Grenfell, B.T., 2004. Stochastic and spatial dynamics of nematode
479 parasites in farmed ruminants. Proceedings of the Royal Society of London. Series B:
480 Biological Sciences 271 (1545), 1243–1250. doi:10.1098/rspb.2004.2744.

481 Courant, R., Friedrichs, K., Lewy, H., 1967. On the partial difference equations of mathe-
482 matical physics. IBM Journal 11 (2), 215–234. doi:10.1147/rd.112.0215.

483 Couzin, I.D., Krause, J., James, R., Ruxton, G.D., Franks, N.R., 2002. Collective memory
484 and spatial sorting in animal groups. Journal of Theoretical Biology 218 (1), 1–11. doi:
485 10.1006/jtbi.2002.3065.

486 Dobson, A., Molnár, P.K., Kutz, S., 2015. Climate change and Arctic parasites. Trends in
487 Parasitology 31 (5), 181–188. doi:10.1016/j.pt.2015.03.006.

488 Dobson, A.P., Hudson, P.J., 1992. Regulation and stability of a free-living host-parasite
489 system: *Trichostrongylus tenuis* in red grouse. II. Population models. Journal of Animal
490 Ecology 61, 487–498.

491 Eftimie, R., de Vries, G., Lewis, M.a., Lutscher, F., 2007. Modeling Group Formation and
492 Activity Patterns in Self-Organizing Collectives of Individuals. Bulletin of Mathematical
493 Biology 69 (5), 1537–1565. doi:10.1007/s11538-006-9175-8.

494 Ferguson, M.A.D., Williamson, R.G., Messier, F., 1998. Inuit Knowledge of Long-Term
495 Changes in a Population of Arctic Tundra Caribou. Arctic 51 (3), 201–219.

496 Folstad, I., Nilssen, A.C., Halvorsen, O., Andersen, J., 1991. Parasite avoidance: the cause
497 of post-calving migrations in Rangifer? Canadian Journal of Zoology 69, 2423–2429.

498 Hall, R.J., Altizer, S., Bartel, R.A., 2014. Greater migratory propensity in hosts lowers
499 pathogen transmission and impacts. Journal of Animal Ecology 83, 1068–1077. doi:
500 10.1111/1365-2656.12204.

Hall, R.J., Brown, L.M., Altizer, S., 2016. Modeling vector-borne disease risk in migratory animals under climate change. Integrative and Comparative Biology 56 (2), icw049. doi: 10.1093/icb/icw049.

Hudson, P., Greenman, J., 1998. Competition mediated by parasites: Biological and theoretical progress. Trends in Ecology and Evolution 13 (10), 387–390. doi:10.1016/S0169-5347(98)01475-X.

Hudson, P.J., Rizzoli, A.P., Grenfell, B.T., Heesterbeek, J.A.P., Dobson, A.P., 2002. Ecology of wildlife diseases. Oxford University Press.

Hundsdorfer, W., Verwer, J.G., 2013. Numerical solution of time-dependent advection-diffusion-reaction equations, volume 33. Springer Science & Business Media.

Johns, S., Shaw, A.K., 2015. Theoretical insight into three disease-related benefits of migration. Population Ecology 58, 213. doi:10.1007/s10144-015-0518-x.

Kretzschmar, M., Adler, F.R., 1993. Aggregated distributions in models for patchy populations. Theoretical Population Biology 43, 1–30.

Krkošek, M., Connors, B.M., Ford, H., Peacock, S., Mages, P., Ford, J.S., Morton, A., Volpe, J.P., Hilborn, R., Dill, L.M., Lewis, M.A., 2011. Fish farms, parasites, and predators: implications for salmon population dynamics. Ecological Applications 21 (3), 897–914. doi:10.1890/09-1861.1.

Krkošek, M., Gottesfeld, A., Proctor, B., Rolston, D., Carr-Harris, C., Lewis, M.A., 2007. Effects of host migration, diversity and aquaculture on sea lice threats to Pacific salmon populations. Proceedings of the Royal Society B 274 (1629), 3141–3149. doi:10.1098/rspb.2007.1122.

Kutz, S.J., Checkley, S., Verocai, G.G., Dumond, M., Hoberg, E.P., Peacock, R., Wu, J.P., Orsel, K., Seegers, K., Warren, A.L., Abrams, A., 2013. Invasion, establishment, and

range expansion of two parasitic nematodes in the canadian arctic. Global Change Biology 19 (11), 3254–3262. doi:10.1111/gcb.12315.

Lutscher, F., 2002. Modeling alignment and movement of animals and cells. Journal of Mathematical Biology 45 (3), 234–260. doi:10.1007/s002850200146.

May, R.M., 1978. Host-Parasitoid Systems in Patchy Environments: A Phenomenological Model. Journal of Animal Ecology 47 (3), 833–844.

May, R.M., Anderson, R.M., 1991. Infectious Diseases of Humans. Oxford University Press, Oxford.

Milner, F.A., Zhao, R., 2008. A deterministic model of schistosomiasis with spatial structure. Mathematical Biosciences and Engineering 5 (3), 505–522. doi:10.3934/mbe.2008.5.505.

Morgan, E.R., Medley, G.F., Torgerson, P.R., Shaikenov, B.S., Milner-Gulland, E.J., 2007. Parasite transmission in a migratory multiple host system. Ecological Modelling 200 (3-4), 511–520. doi:10.1016/j.ecolmodel.2006.09.002.

Nendick, L., Sackville, M., Tang, S., Brauner, C.J., Farrell, A.P., 2011. Sea lice infection of juvenile pink salmon (*Oncorhynchus gorbuscha*): effects on swimming performance and postexercise ion balance. Canadian Journal of Fisheries & Aquatic Sciences 68 (2), 241–249. doi:10.1139/F10-150.

Pruvot, M., Lejeune, M., Kutz, S., Hutchins, W., Musiani, M., Massolo, A., Orsel, K., 2016. Better Alone or in Ill Company? The Effect of Migration and Inter-Species Comingling on Fascioloides magna Infection in Elk. Plos One 11 (7), e0159319. doi:10.1371/journal.pone.0159319.

Qviller, L., Risnes-Olsen, N., Bærum, K.M., Meisingset, E.L., Loe, L.E., Ytrehus, B., Viljugrein, H., Mysterud, A., 2013. Landscape Level Variation in Tick Abundance Relative to Seasonal Migration in Red Deer. PLoS ONE 8 (8). doi:10.1371/journal.pone.0071299.

549 Redpath, S.M., Mougeot, F., Leckie, F.M., Elston, D.A., Hudson, P.J., 2006. Testing the
550 role of parasites in driving the cyclic population dynamics of a gamebird. Ecology Letters
551 9 (4), 410–418. doi:10.1111/j.1461-0248.2006.00895.x.

552 Riley, S., Eames, K., Isham, V., Mollison, D., Trapman, P., 2015. Five challenges for spatial
553 epidemic models. Epidemics 10, 68–71. doi:10.1016/j.epidem.2014.07.001.

554 Risely, A., Klaassen, M., Hoye, B.J., 2017. Migratory animals feel the cost of getting sick: a
555 meta-analysis across species. Journal of Animal Ecology In press. doi:10.1111/ijlh.12426.

556 Salsa, S., 2015. Partial differential equations in action, volume 86. Springer-Verlag, Milan,
557 Italy, second edition. doi:10.1007/978-3-319-15093-2.

558 Satterfield, D.A., Maerz, J.C., Altizer, S., 2015. Loss of migratory behaviour increases
559 infection risk for a butterfly host. Proceedings of the Royal Society B: Biological Sciences
560 282, 20141734. doi:10.1098/rspb.2014.1734.

561 Shaw, D.J., Grenfell, B.T., Dobson, A.P., 1998. Patterns of macroparasite aggregation in
562 wildlife host populations. Parasitology 117, 597–610. doi:10.1017/S0031182098003448.

563 Wilcove, D.S., Wikelski, M., 2008. Going, going, gone: Is animal migration disappearing?
564 PLoS Biology 6 (7), 1361–1364. doi:10.1371/journal.pbio.0060188.

Appendix A. Well posedness and positivity

In this appendix, we prove the well posedness and positivity of the solution to equations (1-5) and show the existence of N, m, and A and their moving counterparts. We start by considering the problem posed by equations (1-5), but instead of considering i up to an infinite number of parasites, we assume that the number of parasites per host is bounded by some large number I (e.g., the carrying capacity for macroparasites on hosts). Equations (1-5) then become:

$$\begin{cases} \frac{\partial p_0}{\partial t} & = \beta \sum_{i=0}^{I}(p_i + \hat{p}_i) - (\mu + \lambda L + \omega)p_0 + \sigma p_1 + \gamma \hat{p}_0 \\ \frac{\partial p_i}{\partial t} & = (\lambda L + \rho(i-1))p_{i-1} - (\mu + \lambda L + i(\alpha + \sigma + \rho) + \omega)p_i + \sigma(i+1)p_{i+1} + (\gamma + i\theta)\hat{p}_i \\ \frac{\partial p_I}{\partial t} & = (\lambda L + \rho(I-1))p_{I-1} - (\mu + \lambda L + I(\alpha + \sigma + \rho) + \omega)p_I + (\gamma + I\theta)\hat{p}_I \\ \frac{\partial \hat{p}_0}{\partial t} + c\frac{\partial \hat{p}_0}{\partial x} & = \omega p_0 - (\mu + \lambda L + \gamma)\hat{p}_0 + \sigma \hat{p}_1 \\ \frac{\partial \hat{p}_i}{\partial t} + c\frac{\partial \hat{p}_i}{\partial x} & = (\lambda L + \rho(i-1))\hat{p}_{i-1} - (\mu + \lambda L + i(\alpha + \sigma + \rho) + \gamma + i\theta)\hat{p}_i + \omega p_i + \sigma(i+1)\hat{p}_{i+1} \\ \frac{\partial \hat{p}_I}{\partial t} + c\frac{\partial \hat{p}_I}{\partial x} & = (\lambda L + \rho(I-1))\hat{p}_{I-1} - (\mu + \lambda L + I(\alpha + \sigma + \rho) + \gamma + I\theta)\hat{p}_I + \omega p_I \\ \frac{\partial L}{\partial t} & = \kappa \sum_{i=1}^{I} i(p_i + \hat{p}_i) - \mu_L L - \lambda L \sum_{i=0} I p_i + \hat{p}_i \end{cases} \tag{A.1}$$

for all $x \in \Omega = \mathbb{R}$, $t > 0$, $i \in \{1, \ldots, I-1\}$, for some $I \in \mathbb{N}$ large enough, with the initial conditions $p_i(0,x) = p_i^0(x)$, $\hat{p}_i(0,x) = \hat{p}_i^0(x)$, and $L(0,x) = L^0(x)$ given for all $i \in \{0, \ldots, I\}$ such that p_i^0, $\hat{p}_i^0$ and L^0 are non-negative, continuously differentiable, and integral in $\mathbb{R}$. More assumptions on the positivity of the initial conditions follow.

First, we prove the local existence of problem (A.1) and the uniqueness of a maximal solution, satisfying the initial condition (and boundary condition, when needed) using classical arguments as in Salsa (2015, Section 11.2.2) and Lutscher (2002). Then we prove that when they exist, the solutions are non-negative (assuming the initial conditions are non-negative) and can not blow up in time. This will prove the existence and uniqueness of a global solution. Using the Gronwall Lemma, we prove that each p_i is bounded from below by an

exponential function in time, which proves that as soon as the initial condition is positive, the solution is positive for all time. We then deduce that $N > 0$, $\hat{N} > 0$, $P > 0$ $\hat{P} > 0$ and m, $\hat{m}$, A, and $\hat{A}$ are well defined for all time.

Appendix A.1. Existence and uniqueness of the solutions for small time

Using the methods of characteristics and the Banach fixed point theorem (see Section 11.2.2 of Salsa, 2015; Lutscher, 2002), we prove that there exists a smooth solution $(p_0, p_1, \ldots, p_I, \hat{p}_0, \ldots, \hat{p}_I, L)$ defined on some interval $[0, T_1]$ for T_1 small enough.

One starts by considering the problem along the characteristics. To make things clearer we will denote by $\underline{u} = (u_0, \ldots, u_I, u_{I+1}, \ldots, u_{2I+1}, u_{2I+2}) = (p_0, \ldots, p_I, \hat{p}_0, \ldots, \hat{p}_I, L)$ and define $\underline{c} = (c_0, \ldots, c_{2I+2}) = (0, \ldots, 0, c, \ldots, c, 0)$ as the migration speed associated with each u_i. Now for each $i \in \{0, \ldots, 2I + 2\}$, let $x_i(t) = \underline{c}_i t + \text{constant}$. Then, denoting $v_i(t) := u_i(t, x_i(t))$, v_i solves the following ODE:

$$\dot{v_i} = f_i(\underline{u}(t, x_i(t))) \tag{A.2}$$

with f_i being the reaction term of u_i in problem (A.1). The $\cdot$ on v_i stands for the derivative with respect to time. Integrating equation (A.2) with respect to time, we obtain for each i

$$u_i(t, x_i(t)) = u_i(0, x_i(0)) + \int_0^t f(\underline{u}(s, x_i(s)))ds. \tag{A.3}$$

Notice that this argument can be adapted if $x \in \Omega \subsetneq \mathbb{R}$ and instead of going from 0 to t on the right hand side above, we will go from t_0 to t with $x_i(t_0)$ on the left boundary of the domain (as the population migrate from left to right).

Let $C^0((0, T_1), B(u^0, \beta))$ be the set of continuous function defined for all $t \in [0, T_1]$, taking its values in the ball centred at u^0, a continuous function, with radius $\beta > 0$. Then the second step is to prove that there exists some β, $T_1 > 0$ such that if $\underline{u} \in \left(C^0((0, T_1), B(u^0, \beta)\right)^m$, with $m = 2I + 2$, then the right hand side of (A.3) also belongs to $\left(C^0((0, T_1), B(u^0, \beta)\right)^m$.

We know that f is locally Lipschitz, thus for all $u_0 \in (B(0,\beta))^m$ and $u \in \big(B(u^0,\beta)\big)^m$, there exists $k_\beta > 0$ such that

$$||f(\underline{u})|| \leq k_\beta ||\underline{u}|| \leq k_\beta \cdot 2\beta := M. \tag{A.4}$$

Choose $T_1 = \beta/M (= 1/(2 \cdot k_\beta)$, then for all $t \in (0, T_1)$,

$$u_i(0, x_i(0)) + \int_0^t f(\underline{u}(s, x_i(s)))ds \in B(u^0, \beta). \tag{A.5}$$

Moreover, with the same choice of T_1 above, one can prove that $u \mapsto u(0, x_i(0)) + \int_0^t f(u(s, x(s)))$ is a contraction. Using the Banach fixed point theorem, we obtain the existence and uniqueness of the maximal solution of problem (A.1) defined for all $t \in (0, T)$, for some $T > 0$ and $x \in \mathbb{R}$ (or $\Omega \subsetneq \mathbb{R}$).

One has thus proved the existence and uniqueness of a maximal *mild* solution of our problem defined for all $t \in (0, T)$, for some $T > 0$, and for all $x \in \mathbb{R}$. To prove the existence of a classical solution (that is, a solution in C^1), one can use the same argument with the initial condition (and boundary condition if $\Omega \subsetneq \mathbb{R}$) in C^1 and $f \in C^{1,1}_{\text{loc}}$ and prove that the solution is integrable on $\mathbb{R}$ for all $t \in (0, T)$, for some $T > 0$ (as we assumed that the initial condition is integrable). Now one needs to prove that the solution of problem (A.1) exists for all time $t \in \mathbb{R}^+$, that is the solution can not blow up in finite time.

Appendix A.2. Existence, uniqueness, and non-negativity of the solutions for all time

First notice that all the components of the problem u_i, $i \in \{0, \ldots, 2I + 2\}$ stay non-negative if the initial condition is non-negative. Indeed, if u_i touches 0 and all the other functions u_j, $j \neq i$ stay non-negative, then $\frac{d}{dt} u_i(t, x_i(t)) \geq 0$ and thus u_i stays non-negative. This argument can be applied to all u_i, $i \in \{0, \ldots, 2I + 2\}$ to prove the non-negativity of our system.

Now one can study the behaviour of the total abundance of hosts at (x,t), considering

$$\bar{N} = \sum_{i=0}^{I} p_i + \hat{p}_i \tag{A.6}$$

and then

$$\bar{\bar{N}}(t) = \int_\Omega \bar{N}(t,x)dx < \infty \tag{A.7}$$

Summing and integrating the PDEs from (A.1) we obtain that

$$\begin{aligned}\frac{d\bar{\bar{N}}}{dt} = &- \int_\Omega \underline{c} \cdot \sum_{i=0}^{I} \partial_x \hat{p}_i(t,x)dx \\ &- \int_\Omega (\mu - \beta) \sum_{i=0}^{I} (p_i(t,x) + \hat{p}_i(t,x))dx \\ &- \int_\Omega \left[(\lambda L + I\rho)(p_I(t,x) + \hat{p}_I(t,x)) + \alpha \sum_{i=1}^{I} i(p_i(t,x) + \hat{p}_i(t,x)) \right] dx \end{aligned} \tag{A.8}$$

Using the regularity of the solution, we know that for all $t \in \mathbb{R}^+$, $-\int_\Omega \underline{c} \cdot \sum_{i=0}^{I} \partial_x \hat{p}_i(t,x)dx = 0$, when $\Omega = \mathbb{R}$. In the case of bounded domain, for Dirichlet boundary conditions or periodic boundary conditions, the first term on the right-hand side is equal to or less than zero and because of the non-negativity of the solution we get

$$\frac{d\bar{\bar{N}}}{dt} \leq -(\mu - \beta)\bar{\bar{N}}(t). \tag{A.9}$$

Using Gronwall Lemma we obtain that

$$\bar{\bar{N}}(t) \leq \bar{\bar{N}}(0)e^{-(\mu-\beta)t} \tag{A.10}$$

which yields, for each $i \in \{0, \ldots, 2I+1\}$, $u_i(t,x) \leq \bar{\bar{N}}(0)e^{-(\mu-\beta)t}$ for all $t \geq 0$, $x \in \Omega$. This proves that the solution of problem (A.1) can not blow up in time and it is thus global in time, in the sense that there exists a unique maximal solution of problem (A.1) that exists

for all $t > 0$, $x \in \Omega$.

Moreover, notice that as soon as $\beta < \mu$ we obtain that $\bar{\bar{N}}$ is decreasing in time and thus for all $i \in \{0, \dots, 2I+1\}$

$$u_i(t,x) \leq \bar{\bar{N}}(0) \tag{A.11}$$

That is for all $i \in \{0, \dots, I\}$, p_i and $\hat{p}_i$ are bounded for all $t \geq 0$, $x \in \Omega$.

Appendix A.3. Positivity of the solutions

Using the same argument as in previous subsection, we can prove that for all $t > 0$, $x \in \Omega$

$$L(t,x) \leq f(t) \tag{A.12}$$

with f being a positive function defined for all $t > 0$. Then using equations (A.1) we obtain for each $i \in \{0, \dots, I\}$,

$$\frac{\partial p_i}{\partial t} \geq -(\mu + f(t) + i(\alpha + \sigma + \rho) + \omega)p_i \tag{A.13}$$

and

$$\frac{d\hat{p}_i}{dt}(t, ct + x_0) \geq -(\mu + f(t) + i(\alpha + \sigma + \rho) + \gamma + i\theta)\hat{p}_i(t, ct + x_0). \tag{A.14}$$

Using the Gronwall lemma once again, we obtain that for all $i \in \{0, \dots, I\}$,

$$p_i(t,x) \geq e^{-\int_0^t \mu + f(s) + i(\dots) + \omega) ds} p_i(0,x) > 0 \tag{A.15}$$

and

$$\hat{p}_i(t, ct + x_0) \geq e^{-\int_0^t \mu + f(s) + i(\dots) + \gamma + i\theta) ds} \hat{p}_i(0, x_0) > 0 \tag{A.16}$$

for all $t > 0$, $x \in \Omega$. This proves that as soon as the initial condition is positive, the solution is positive for all $t > 0$. Then the total population of stationary hosts $N_I(t,x) := \sum_{i=0}^{I} p_i$ is positive, the total population of moving hosts $\hat{N}_I(t,x) := \sum_{i=0}^{I} \hat{p}_i$ is positive, the total

population of parasites in/on stationary hosts $P_I(t,x) := \sum_{i=0}^{I} i p_i$ is positive, and the total population of parasites in/on moving hosts is $\hat{P}_I(t,x) := \sum_{i=0}^{I} i \hat{p}_i(t,x)$ is positive.

Appendix A.4. System with N, m and A and their migratory counterpart

Considering $N_I := \sum_{i=0}^{I} p_i$, $P_I := \sum_{i=0}^{I} i p_i$ and $Q_I = \sum_{i=0}^{I} i^2 p_i$ (see Appendix B for the definition of Q), we obtain the following system of partial differential equations for N_I, P_I, Q_I and their moving counterparts (we omit the subscript I for N, P and Q and their moving counterparts for simplicity of notation):

$$
\begin{cases}
\frac{\partial N}{\partial t} & = \beta(N+\hat{N}) - (\mu+\omega)N - \alpha P + \gamma \hat{N} + \theta \hat{P} \\
& \quad -\mathbf{p_I}(\lambda \mathbf{L} + \mathbf{p}) \\
\frac{\partial P}{\partial t} & = \lambda L N - (\mu+\omega+\sigma-\rho)P - \alpha Q + \gamma \hat{P} + \theta \hat{Q} \\
& \quad -\mathbf{p_I}(\lambda \mathbf{L}(\mathbf{1}+\mathbf{I}) + \rho(\mathbf{I^2}+\mathbf{I})) \\
\frac{\partial Q}{\partial t} & = (\lambda L - \alpha g'''(1))N + (\sigma + 2\lambda L + 2\alpha + \rho)P \\
& \quad - (\mu + 2\sigma + \omega + 3\alpha - 2\rho) + \theta \hat{g}'''(1)\hat{N} - 2\theta \hat{P} + (\gamma + 3\theta)\hat{Q} \\
& \quad -\mathbf{p_I}(\lambda \mathbf{L}(\mathbf{I^2}+\mathbf{2I}+\mathbf{1}) + \rho(\mathbf{I^3}+\mathbf{2I}+\mathbf{I})) \\
\frac{\partial \hat{N}}{\partial t} + c\frac{\partial \hat{N}}{\partial x} & = \omega N - (\mu+\gamma)\,\hat{N} - (\alpha+\theta)\hat{P} \\
& \quad -\mathbf{p_I}(\dots) \\
\frac{\partial \hat{P}}{\partial t} + c\frac{\partial \hat{P}}{\partial x} & = \omega P + (\lambda L - (\alpha+\theta)\hat{g}'''(1))\hat{N} - (\mu+\sigma+\gamma-2(\alpha+\theta)-\rho)\hat{P} - 3(\alpha+\theta)\hat{Q} \\
& \quad -\mathbf{p_I}(\dots) \\
\frac{\partial \hat{Q}}{\partial t} + c\frac{\partial \hat{Q}}{\partial x} & = \omega Q + (\lambda L - (\alpha+\theta)\hat{g}'''(1))\hat{N} + (\sigma + 2\lambda L + 2(\alpha+\theta) + \rho)\hat{P} \\
& \quad - (\mu + 2\sigma + \gamma + 3(\alpha+\theta) - 2\rho)\hat{Q} \\
& \quad -\mathbf{p_I}(\dots) \\
\frac{\partial L}{\partial t} & = \kappa(P+\hat{P}) - \mu_L L - \lambda L(N+\hat{N})
\end{cases}
\tag{A.17}
$$

Because the sums are finite, we end up with some extra terms depending on I and p_I, highlighted in bold, which do not appear in the main problem (14 - 19). However, assuming that for all $n \in \mathbb{N}$,

$$\lim_{I\to+\infty} \sum_{i=0}^{I} i^n p_i \text{ and } \lim_{I\to+\infty} \sum_{i=0}^{I} i^n \hat{p}_i \tag{A.18}$$

exist for all $t > 0$, $x \in \Omega$, we can define $N_\infty := \lim_{I\to+\infty} N_I$, $P_\infty := \lim_{I\to+\infty} P_I$, $Q_\infty := \lim_{I\to+\infty} Q_I$, and their moving counterparts. This assumption roughly means that the distribution of parasites among hosts has finite moment, which is true, for instance, for the Poisson or negative binomial distributions. This assumption was implicitly made (at least up to $n = 3$) in Kretzschmar and Adler (1993). From this assumption we also obtain that for I large enough and for all $n \in \mathbb{N}$,

$$p_I < I^{-n} << 1 \tag{A.19}$$

and thus when I is large enough, system (A.17) can be approximated by

$$\begin{cases} \frac{\partial N}{\partial t} & = \beta(N+\hat{N}) - (\mu+\omega)N - \alpha P + \gamma\hat{N} + \theta\hat{P} \\ \frac{\partial P}{\partial t} & = \lambda L N - (\mu+\omega+\sigma-\rho)P - \alpha Q + \gamma\hat{P} + \theta\hat{Q} \\ \frac{\partial Q}{\partial t} & = (\lambda L - \alpha g'''(1))N + (\sigma + 2\lambda L + 2\alpha + \rho)P \\ & \quad - (\mu + 2\sigma + \omega + 3\alpha - 2\rho) + \theta\hat{g}'''(1)\hat{N} - 2\theta\hat{P} + (\gamma+3\theta)\hat{Q} \\ \frac{\partial \hat{N}}{\partial t} + c\frac{\partial \hat{N}}{\partial x} & = \omega N - (\mu+\gamma)\,\hat{N} - (\alpha+\theta)\hat{P} \\ \frac{\partial \hat{P}}{\partial t} + c\frac{\partial \hat{P}}{\partial x} & = \omega P + (\lambda L - (\alpha+\theta)\hat{g}'''(1))\hat{N} - (\mu+\sigma+\gamma-2(\alpha+\theta)-\rho)\hat{P} - 3(\alpha+\theta)\hat{Q} \\ \frac{\partial \hat{Q}}{\partial t} + c\frac{\partial \hat{Q}}{\partial x} & = \omega Q + (\lambda L - (\alpha+\theta)\hat{g}'''(1))\hat{N} + (\sigma + 2\lambda L + 2(\alpha+\theta) + \rho)\hat{P} \\ & \quad - (\mu + 2\sigma + \gamma + 3(\alpha+\theta) - 2\rho)\hat{Q} \\ \frac{\partial L}{\partial t} & = \kappa(P+\hat{P}) - \mu_L L - \lambda L(N+\hat{N}) \end{cases} \tag{A.20}$$

which yields problem (14-19).

Appendix B. Derivation of dynamic equations for the VMR

Following the derivation of the non-spatial model of Kretzschmar and Adler (1993), we introduce a third aggregate variable, $Q = \sum i^2 p_i$ (and its migratory counterpart, $\hat{Q}$). The following equations describing the change in Q and $\hat{Q}$ were found by multiplying equations (1-4) by i^2 and summing (as for P and $\hat{P}$):

$$\frac{\partial Q}{\partial t} = -(\mu + 2\sigma + \omega)Q + (\sigma + 2\phi)P + \phi N + \gamma\hat{Q} - \alpha N \sum_{i=0}^{\infty} i^3 r_i + \theta\hat{N} \sum_{i=0}^{\infty} i^3 \hat{r}_i \quad \text{(B.1)}$$

$$\frac{\partial \hat{Q}}{\partial t} - c\frac{\partial \hat{Q}}{\partial x} = -(\mu + 2\sigma + \gamma)\hat{Q} + (\sigma + 2\phi)\hat{P} + \phi\hat{N} + \omega Q - (\alpha + \theta)\hat{N} \sum_{i=0}^{\infty} i^3 \hat{r}_i. \quad \text{(B.2)}$$

Applying the chain rule as above, we can get equations for $u = Q/N$ and $\hat{u} = \hat{Q}/\hat{N}$. We can use a trick with probability generating functions to deal with the sums in equations (B.1-B.2). The sums can be expressed as:

$$\sum_{i=0}^{\infty} i^3 r_i = g'''(1) + 3u - 2m, \quad \text{(B.3)}$$

where $g(z)$ is the probability generating function of the distribution of r_i (e.g., the negative binomial distribution), and $g'''(1)$ is the third derivative evaluated at $z = 1$ (see Appendix II of Kretzschmar and Adler (1993)). Inserting equation (B.3) into equations (B.1-B.2) and solving for $\partial u/\partial t$ and $\partial \hat{u}/\partial t - c\,\partial \hat{u}/\partial x$, we get

$$\frac{\partial u}{\partial t} = -\,u\left(2\sigma + \beta\left(\frac{N+\hat{N}}{N}\right)\right) + m(\sigma+2\phi) + \phi - \alpha(g'''(1) + 3u - 2m - um) \tag{B.4}$$

$$+\,\frac{\hat{N}}{N}\Big[\theta\left(\hat{g}'''(1) + 3\hat{u} - 2\hat{m} - \hat{m}u\right) + \gamma(\hat{u}-u)\Big]$$

$$\frac{\partial \hat{u}}{\partial t} - c\frac{\partial \hat{u}}{\partial x} = \hat{u}\Big(\hat{m}(\alpha+\theta) - 2\sigma\Big) + \hat{m}(\sigma+2\phi) + \phi + \omega\frac{N}{\hat{N}}(u-\hat{u}) \tag{B.5}$$

$$-\,(\alpha+\theta)(\hat{g}'''(1) + 3\hat{u} - 2\hat{m})$$

677 The VMR, A, can be expressed in terms of u and m:

$$A = \frac{\text{variance}}{m} = \frac{\sum_{i=0}^{\infty} i^2 r_i - m^2}{m} = \frac{u - m^2}{m}. \tag{B.6}$$

678 We can use equation (B.6) to obtain a differential equation for A of the form:

$$\frac{\partial A}{\partial t} = \frac{1}{m}\frac{\partial u}{\partial t} - \frac{u}{m^2}\frac{\partial m}{\partial t} - \frac{\partial m}{\partial t}. \tag{B.7}$$

679 Using equations (B.1-B.2), (15), and (17), and substituting $u = m(A+m)$ and $\hat{u} = \hat{m}(\hat{A}+\hat{m})$,

680 we can write the equations for the change in the VMR:

$$\frac{\partial A}{\partial t} = \beta m \left(\frac{N+\hat{N}}{N}\right) - (A-1)\left(\sigma + \frac{\phi}{m}\right)$$
$$- \alpha\left(\frac{g'''(1)}{m} + 3(A+m) - (2+m(A+m)) - A(A+2m)\right)$$
$$+ \frac{\hat{N}}{Nm}\Bigg[\theta\Big(\hat{g}'''(1) + 3\hat{m}(\hat{A}+\hat{m}) - \hat{m}(2+m(A+m)) - \hat{m}(\hat{A}+\hat{m}-m)\,(A+2m)\Big)$$
$$+\ \gamma\Big(\hat{m}(\hat{A}+\hat{m}) - m(A+m) - (A+2m)(\hat{m}-m)\Big)\Bigg] \tag{B.8}$$

$$\frac{\partial \hat{A}}{\partial t} - c\frac{\partial \hat{A}}{\partial x} = (\alpha+\theta)\left[\hat{A}(3\hat{m}-3+\hat{A}) + \hat{m}(\hat{m}-3) + 2 - \frac{\hat{g}'''(1)}{\hat{m}}\right]$$
$$- (\hat{A}-1)\left(\sigma + \frac{\phi}{\hat{m}}\right) + \omega\frac{Nm}{\hat{N}\hat{m}}\left(A + m + \frac{\hat{m}^2}{m} - \hat{A} - 2\hat{m}\right) \tag{B.9}$$

To apply the model in equations (14-17) and (B.8-B.9), we need to define $g'''(1)$ and $\hat{g}'''(1)$ by assuming a distribution of parasites among hosts. Defining the distribution still allows for the mean and VMR in the parasite burden to change in space and time, thus accounting for changes in the overdispersion.

If we assume that parasites are distributed among hosts according to the negative binomial, then we can make the substitutions:

$$g'''(1) = m(m+A-1)(m+2(A-1))$$
$$\hat{g}'''(1) = \hat{m}(\hat{m}+\hat{A}-1)(\hat{m}+2(\hat{A}-1)) \tag{B.10}$$

These substitutions simplify equations (B.8-B.9), yielding equations (18-19).

Appendix C. Numerical methods

We numerically simulated model solutions on a discrete space-time grid where:

$$x \rightarrow x_i \in \{x_0, x_1, \ldots, x_{n_x}\}$$
$$t \rightarrow t_k \in \{t_0, t_1, \ldots, t_{n_t}\}.$$

We set the grid spacing in the spatial domain, Δx, based on the length of the migration route being considered such that n_x was reasonably large but still computationally feasible. We then chose a sufficiently small time step that densities did not move more than one grid space to avoid numerical errors (i.e., the Courant-Friedrichs-Lewy condition; Courant et al., 1967). In general, the time step should be set to $\Delta t \approx \nu \Delta x / c$, where $0 \leq \nu \leq 1$ is the Courant number and c is the migration speed. Note that if Δt is exactly $\Delta x / c$, then the numerical approximation to the advection equation (step 1 below) is exact. This was the case for our general simulations where we chose a migration speed of $c = 10000$ km yr^{-1} (Table 2), $\Delta x = 1$ km, $\Delta t = 0.0001$ yr, and $\nu = 1$. By using the exact solution, we avoided the effect of "numerical diffusion", whereby the numerical approximation of advection results in a spreading out of the population densities. We denote the numerical approximation of $\hat{N}(x_i, t_k)$ at point (i, k) on the grid as $\hat{N}_{i,k}$.

At each time step in the numerical simulation of the model, we split the model equations into an advection processes, consisting of movement of migratory populations, and a reaction process, consisting of temporal change in population densities, consisting of host birth/death, parasite attachment/death, and switching status between migratory and stationary. As an example, equation (16) can be written as:

$$\frac{\partial \hat{N}}{\partial t} = \underbrace{c \frac{\partial \hat{N}}{\partial x}}_{\mathcal{A}} \underbrace{- \Big(\mu + \gamma + (\alpha + \theta) \hat{m} \Big) \hat{N} + \omega N}_{\mathcal{R}}$$

where $\mathcal{A}$ is the advection process and $\mathcal{R}$ is the reaction process.

We assumed Neumann boundary conditions where the derivative across the boundary is zero. This was simulated by adding a ghost node onto either end of our spatial grid, at $i = -1$ and $i = n_x + 1$. The numerical algorithm proceeded as follows. For each time step k in 1 to n_t:

1. Force boundary conditions by setting $\hat{N}_{-1,k} = \hat{N}_{1,k}$ and $\hat{N}_{n_x+1,k} = \hat{N}_{n_x-1,k}$.
2. Solve $\frac{\partial \hat{N_{\mathcal{A}}}}{\partial t} = \mathcal{A}$ with $\hat{N}_{\mathcal{A}}(x_i, 0) = \hat{N}_{i,k}$ on $[0, \Delta t]$ using a finite upstream differencing method (Hundsdorfer and Verwer, 2013).
3. Solve $\frac{\partial \hat{N_{\mathcal{R}}}}{\partial t} = \mathcal{R}$ with $\hat{N}_{\mathcal{R}}(x_i, 0) = \hat{N}_{\mathcal{A}}(x_i, \Delta t)$ on $[0, \Delta t]$ using a fourth-order Runge-Kutta method.
4. Set $\hat{N}_{i,k+1} = \hat{N}_{\mathcal{R}}(x_i, \Delta t)$.

The above scheme is written for $\hat{N}$, but at each step, the algorithm was applied to the other variables as well. Note, however, that for the non-migratory variables N, m, A, and L, $\mathcal{A} = 0$ and thus $N_{\mathcal{A}}(x_i, \Delta t) = N_{i,k}$.